CHARACTERISTICS OF ACTIVE-REGION SOURCES OF SOLAR WIND NEAR SOLAR MAXIMUM

PAULETT C. LIEWER[1], M. NEUGEBAUER[2] and THOMAS ZURBUCHEN[3]
[1]*Jet Propulsion Laboratory, California Institute of Technology, Mail Stop 169-506, Pasadena, CA 91109, U.S.A. (e-mail: paulett.liewer@jpl.nasa.gov)*
[2]*Lunar and Planetary Laboratory, University of Arizona, Tucson, AZ 85721, U.S.A. (e-mail: mneugeb@lpl.arizona.edu,)*
[3]*University of Michigan, Department of Atmospheric, Oceanic and Space Sciences, Ann Arbor, MI 48105, U.S.A. (e-mail: thomasz@umich.edu)*

(Received 23 December 2003; accepted 10 June 2004)

Abstract. Previous studies of the source regions of solar wind sampled by ACE and *Ulysses* showed that some solar wind originates from open magnetic flux rooted in active regions. These solar wind sources were labeled *active-region sources* when the open flux was from a strong field region with no corresponding coronal hole in the NSO He 10830 Å synoptic coronal-hole maps. Here, we present a detailed investigation of several of these active-region sources using ACE and *Ulysses* solar wind data, potential field models of the corona, and solar imaging data. We find that the solar wind from these active-region sources has distinct signatures, e.g., it generally has a higher oxygen charge state than wind associated with helium-10830 Å coronal-hole sources, indicating a hotter source region, consistent with the active region source interpretation. We compare the magnetic topology of the open field lines of these active-region sources with images of the hot corona to search for corresponding features in EUV and soft X-ray images. In most, but not all, cases, a dark area is seen in the EUV and soft X-ray image as for familiar coronal-hole sources. However, in one case no dark area was evident in the soft X-ray images: the magnetic model showed a double dipole coronal structure consistent with the images, both indicating that the footpoints of the open field lines, rooted deep within the active region, lay near the separatrix between loops connecting to two different opposite polarity regions.

1. Introduction

Near the minimum of solar activity, most of the open magnetic flux and solar wind comes from the large polar coronal holes. Wind from the polar coronal holes is fast ($V > 700$ km s^{-1}) and has well-defined properties, e.g., the source region temperature (using the oxygen freezing-in temperature computed from the ratio of O^{7+} to O^{6+} as a proxy) is typically low, $T_O \approx 1.1$ MK (von Steiger *et al.*, 2000; Geiss, Gloeckler, and von Steiger, 1995; Geiss *et al.*, 1995). The slow solar wind associated with the streamer belt has much more variable properties and a higher, more variable oxygen freezing-in temperature, $T_O = 1.4$–2.0 MK (Geiss, Gloeckler, and von Steiger, 1995; Geiss *et al.*, 1995; Zurbuchen *et al.*, 2000; von Steiger *et al.*, 2000). This slow wind may come from open flux at the boundaries of the polar coronal holes, from low-latitude coronal holes, from closed field regions

Solar Physics **223:** 209–229, 2004.

that have recently opened, or from all of those (Wang and Sheeley, 1997; Wang *et al.*, 1998; Neugebauer *et al.*, 1998; Fisk, 2003).

Near the maximum of solar activity, the pattern of solar wind velocity is very complex with no clear separation of fast and slow wind. At both low and high latitudes near solar maximum, *Ulysses* saw successions of slow and moderate speed wind (McComas, Gosling, and Skoug, 2000; McComas *et al.*, 2001). To understand space weather trends, Luhmann *et al.* (2002) analyzed the evolution of the open magnetic flux connecting the Sun to the heliosphere over the last 3 solar cycles using potential field source surface (PFSS) magnetic models computed from Mt. Wilson Observatory synoptic magnetograms. They found that at solar maximum, most open flux comes from low and mid latitudes, in contrast to solar minimum, when most open flux comes from the polar regions. Recent PFSS modeling of the evolution of coronal magnetic fields by Schrijver and DeRosa (2003) has shown that the open flux from active regions (areas with a flux intensity > 50 Mx cm^2) increases from $< 1\%$ at solar minimum to 30–50% at solar maximum. Schrijver and DeRosa (2003) also compared PFSS models of active regions with open flux to TRACE EUV images to verify the connection of open field lines to the active region. Open flux from active regions may contribute to slow wind at solar minimum as well: Kojima *et al.* (1998) using interplanetary scintillation data and potential magnetic field models found that at solar minimum some slow solar wind originated from rapidly expanding open flux associated with one polarity side of an active region.

Mapping *in situ* solar wind data to its solar source region is a useful tool for understanding the origin and structure of the solar wind (Neugebauer *et al.*, 1998 and references therein). A recent mapping study of the solar wind near solar maximum by Neugebauer *et al.* (2002) has shown that open flux associated with active regions is an important source of slow solar wind sampled by the *Advanced Composition Explorer* (ACE) and *Ulysses* and that the wind from such active regions has properties distinct from that of the wind from polar and equatorial coronal hole sources. Neugebauer *et al.* (2002) also found that the interface region between streams from two sources of the *same* magnetic polarity had many features in common with plasma sheet interfaces between streams of opposite polarities. They concluded that there are three types of slow wind near solar maximum (not including transient CMEs): traditional coronal hole wind, active region slow wind, and slow wind in stream interfaces. Wang and Sheeley (2002) found that, at solar maximum, most of the wind sampled by ACE came from regions with strong magnetic fields and large flux tube expansion factors (as in active regions) and that the wind from these regions had properties different from wind from regions of weak magnetic fields and small flux tube expansion factor (consistent with the study of Neugebauer *et al.*, 2002). Both of these mapping studies used a standard two-step mapping procedure with a PFSS model to determine the source regions of the sampled solar wind and both studies were statistical in nature.

Open flux from active regions was studied extensively in the *Skylab* era (Levine, 1977; Levine *et al.*, 1977; Švestka *et al.*, 1977) using magnetic models and soft X-ray images of the corona. In Levine *et al.* (1977), open flux from PFSS coronal models was compared with coronal holes identified solely on the basis of dark areas in soft X-ray images. They found that all major *Skylab* coronal holes in the two solar rotations studied were evident as open field regions in the PFSS models. In addition, they found significant open flux associated with active regions that did not have a corresponding *Skylab* coronal hole, but often later enlarged and developed into one. Also, the active-region open flux was generally between loop systems and often had associated dark features in the *Skylab* soft X-ray images. In that work, no comparison with coronal holes as determined from He 10830 Å images was made. Arge *et al.* (2003) recently used *Yohkoh* SXT soft X-ray data and PFSS magnetic models to study three narrow coronal holes seen in the X-ray images, but not in the He 10830 Å images. These narrow coronal holes are probably the equivalent to the dark corridors between loop systems discussed by Švestka *et al.* (1977) and Levine (1977). The three narrow coronal holes in the Arge *et al.* (2003) study were extension of polar coronal holes, but showed higher ratios of O^{7+}/O^{6+} than seen in the solar wind from polar coronal holes at solar minimum.

The primary new result from Neugebauer *et al.* (2002) (Paper I hereafter) is that by combining the source mapping with analyses of the *in situ* data near solar maximum, it was shown that the solar wind from the identified active region sources has different properties, e.g. higher ratios of O^{7+}/O^{6+}, than wind from identified coronal hole sources. Wind from the active regions sources typically had the ratio $O^{7+}/O^{6+} = 0.1–0.6$ (corresponding to an equilibrium oxygen freezing-in temperature range of $T_O = 1.4–1.9$ MK); coronal hole wind typically had $O^{7+}/O^{6+} < 0.2$, corresponding to $T_O < 1.6$ MK). Because of the importance of this result, we present here a detailed study of the morphology of several of these active region sources and a comparison of the solar wind from the active region sources with wind from traditional low-latitude coronal hole sources. In Paper I, a source was classified as an *active-region source* when the open flux of the sampled wind mapped back to a strong magnetic field region on the surface with no nearby coronal hole identified in the NSO synoptic 10830 Å coronal hole maps. It is known that He 10830 Å is an imperfect diagnostic for determining the footpoints of coronal open flux (Levine, 1982). Because of this, some would argue that open flux sources of solar wind in active regions should also be called coronal holes. However, because the wind from these active-region sources shows different properties than wind from traditional coronal holes (dark, density depletions in the corona), we use the term *active-region sources* for these open flux sources in active regions with no corresponding hole in He 10830 Å synoptic maps. Levine (1982) stressed the importance of keeping a distinction between 'open flux' and 'coronal holes' because the definition of a coronal hole is an observational one.

Specifically, in this paper, we present results from a detailed study of several of the active-region sources used in the statistical study in Paper I from Carrington

rotations 1934, 1953 and 1957. Our study uses potential magnetic field extrapolations from synoptic magnetograms, solar imaging data, and ACE and *Ulysses* solar wind data. In Section 2, we describe the two-step source mapping technique and its validation. In Section 3, we analyze solar wind data from ACE and compare wind from active region sources with wind from traditional coronal hole sources and find distinct signatures. Specifically, we find that the charge state density ratio O^{7+}/O^{6+} is not only higher in the solar wind from active regions, but also shows more variability within the wind stream. In coronal hole wind, the density ratio O^{7+}/O^{6+} varies smoothly across the source, with a minimum of < 0.1 (corresponding to $T_O < 1.4$ MK). Because of the distinct coronal hole O^{7+}/O^{6+} profile (and similarly the oxygen charge state profile) in coronal hole wind, we find that in some cases these signatures can be used to resolve ambiguities in the source mapping. In Section 4, we compare the computed magnetic structure of several active region solar wind sources to soft X-ray and EUV images of the corona to look for signatures of the open flux. We find that the images support the contention that the open flux is rooted in the active regions. In most cases studied, the open flux seems to come from one edge of the active region; a dark corridor can be seen in the coronal images, consistent with Levine *et al.* (1977) and Švestka *et al.* (1977). In one case, however, where there is a double dipole magnetic configuration, the open flux maps to the center of one active region. The soft X-ray images are consistent with this configuration, but there is no corresponding dark feature. Section 5 contains our conclusions and discussions.

2. Determination of Source Regions and Validation

The sources of solar wind sampled by ACE and *Ulysses* are determined using a standard two-step mapping process as in Neugebauer *et al.* (1998). In the first step, the solar wind speed measured at the spacecraft is used to ballistically map the solar wind back to its point of origin, or, footpoint, on a source surface at $R = 2.5\ R_{\rm Sun}$; this assumes that the wind traveled radially at the measured velocity from the source surface to the spacecraft. In the second step, a potential field source surface (PFSS) magnetic field model of the corona, extrapolated from an NSO Kitt Peak synoptic magnetogram (found at *ftp://argo.tuc.noao.edu/kpvt/synoptic/mag/*), is used to trace the solar wind back from its source surface footpoint to the photosphere; this assumes that the wind follows the magnetic field lines in the magnetically dominated corona. Further details can be found in Paper I.

We check each mapping against three criteria: (1) Does the polarity of the magnetic field at the spacecraft agree with the polarity predicted by the mapping? (2) Does the potential field model predict open flux where the NSO He 10830 Å synoptic maps (*ftp://ftp.noao.edu/kpvt/synoptic/choles/*) show coronal holes? (3) Do the solar wind data show evidence of a source region boundary at the locations predicted by the model? Paper I analyzed statistically the mappings for four Car-

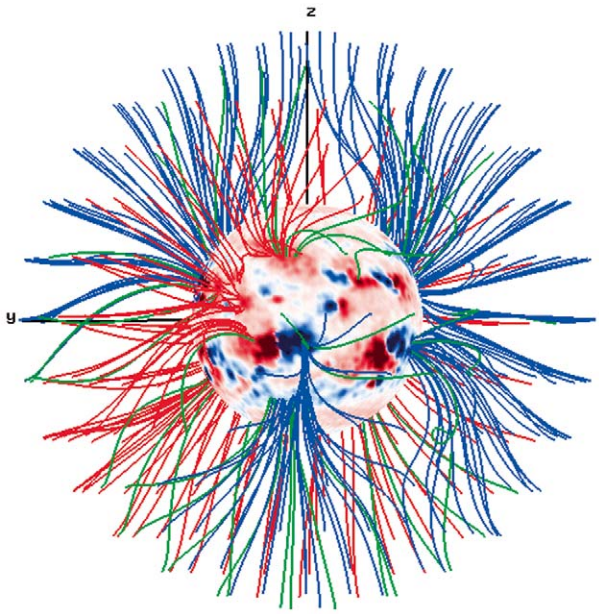

Figure 1. Potential field source surface (PFSS) magnetic field model of the corona for CR1957, as viewed on 18 December 1999. The traced field lines are equally spaced in area at the source surface, $R = 2.5\ R_{\rm Sun}$. *Red (blue) lines* show outward (inward) polarity magnetic field; the *green lines* show the current sheet.

rington rotations where these criteria were generally well satisfied for latitudes equatorward of 60°. Here, we investigate in detail the active-region sources from three of these rotations. A related study of the active-region sources in CR 1934 was presented in Liewer, Neugebauer, and Zurbuchen (2003). While the potential field models generally show the open flux of the He 10830 Å synoptic coronal holes, the models often show additional small regions of open flux in and around active regions with no corresponding He 10830 Å coronal hole in the synoptic maps.

Traced field lines from the PFSS model for CR 1957 (5 December 1999 – 1 January 2000) are shown in Figure 1; the image on the solar sphere is the synoptic magnetogram used to generate the PFSS model. The field lines shown are equally spaced in area at the source surface ($R = 2.5\ R_{\rm Sun}$). Red (blue) lines show outward (inward) polarity magnetic field, and the green lines show the approximate location of the current sheet. Note that much of the open flux in the polar regions originates at middle latitudes. Figure 2 shows the results of the first stage mapping of solar wind from the spacecraft to the source surface ($R = 2.5\ R_{\rm Sun}$). The mapped ACE (in ecliptic) and *Ulysses* (about −40° latitude) data overlie contours of magnetic field at the source surface from the PFSS model for CR 1957. Note the very good agreement between predicted and observed polarities and the current sheet crossings (criterion 1). For this rotation, ACE sees four magnetic sectors while *Ulysses* sees only two. Note also that the current-sheet passes close to both poles of the Sun.

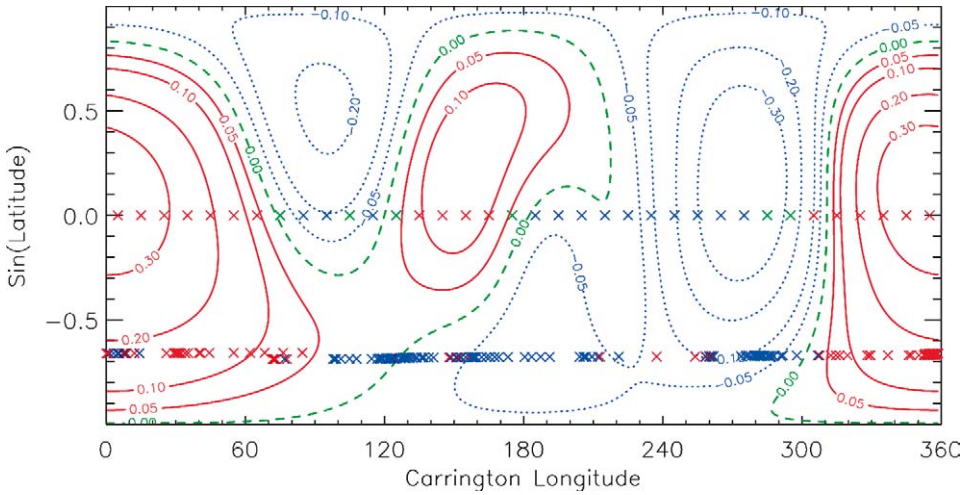

Figure 2. PFSS magnetic contours at the source surface (2.5 R_{Sun}) for CR 1957. *Red (blue) contours* show outward (inward) polarity magnetic field; the *green line* is the current sheet. The ACE (in ecliptic) and *Ulysses* (−40°) data mapped to the source surface are shown as ×'s colored by magnetic field polarity; green ×'s show mixed polarity regions in the spacecraft data. The predicted and observed magnetic polarities are in excellent agreement.

The graph in Figure 3 shows the ballistic relationship between the date on which the solar wind was observed at ACE and the corresponding Carrington longitude on the source surface.

Figure 4 shows the footpoints of the open flux (red and blue ×'s) from the PFSS model shown in Figure 1 compared to the NSO coronal hole map created from the He 10830 Å observations. It can be seen that the model predicts open flux at nearly all synoptic coronal hole locations (second validation criterion). Additional small regions of open flux are predicted by the model, as is typically seen. Figure 5 shows the results for CR 1957 of the second stage mapping of the spacecraft data from the source surface to the Sun's surface tracing PFSS magnetic field lines. The arrow tail is the location at the source surface and the arrow head is at the photosphere (the foot point of the field line). Also shown are the NSO synoptic magnetogram and coronal hole data. Solar wind data taken during coronal mass ejections (CMEs) is not mapped; for a description of how CME periods are determined, see Paper I.

3. Solar Wind Data for Mapped Sources

Note in Figure 5 that the bunching of the arrowheads allows us to easily separate the sampled solar wind into streams from different source regions. In this section, we will look in detail at the solar wind data for three source regions: (1) Some ACE solar wind maps to the strong-field region AR-8798 near 190° longitude; since there is no synoptic coronal hole near this active region, we designate this an

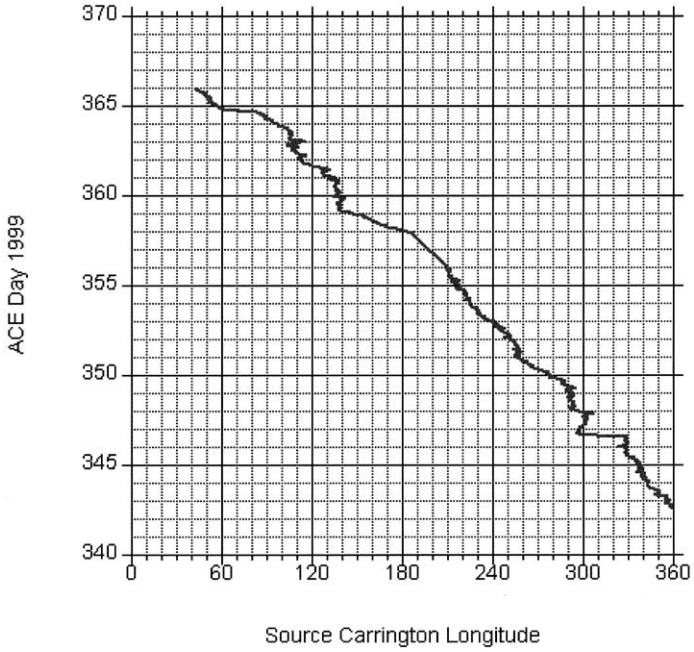

Figure 3. Ballistic relationship between ACE day and source Carrington longitude for CR1957. Note that ACE time decreases with increasing longitude.

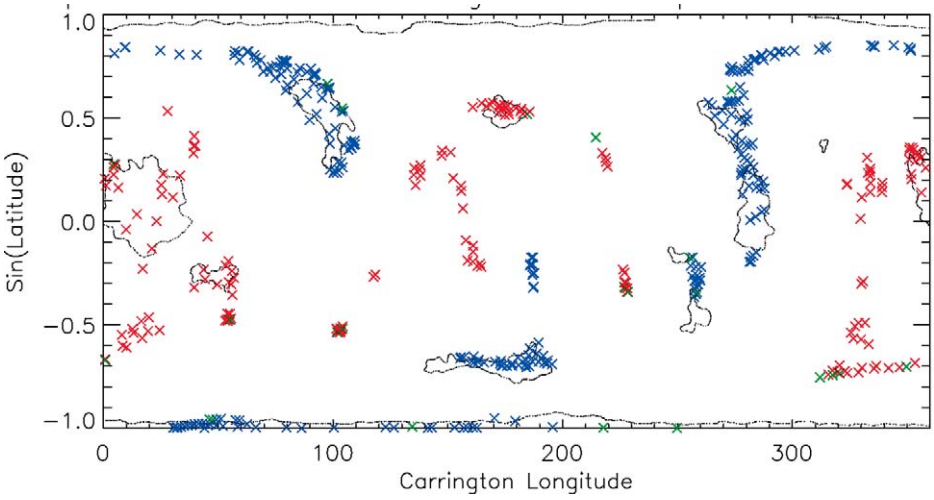

Figure 4. Footpoints of open flux from the CR1957 PFSS magnetic field model of Figure 1 overlying the NSO synoptic coronal hole map contours at the source surface (2.5 R_{Sun}) for CR-1957. The footpoints (+) are colored by polarity-with *red* (*blue*) for outward (inward); the polarity of the NSO coronal holes are denoted by the black + for outward and − for inward. The model shows all equatorial coronal holes seen in the NSO maps and additional areas of open flux as well.

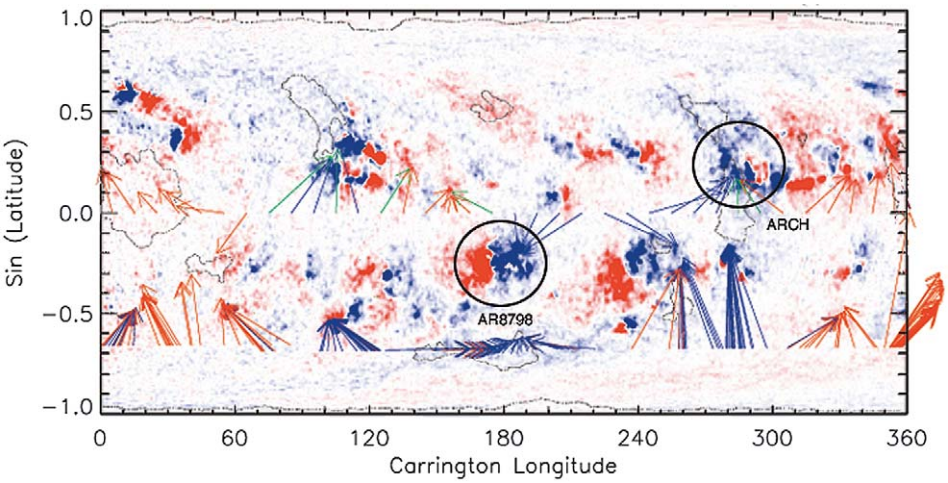

Figure 5. Mapping of spacecraft data from the source surface to the solar surface for CR1957. The arrow tail is the location at the source surface and the head is the footpoint at the solar surface. Also shown are the NSO synoptic magnetogram and coronal hole map. The black + and − denote the polarity of the photospheric field in the coronal holes.

AR (active region) source; (2) some of the ACE wind maps to the large equatorial coronal hole centered at about 10° longitude and we identify this as CH (coronal hole) wind; and (3) some of the ACE wind maps to the strong field region at about 280° longitude straddled by two synoptic coronal holes. There is an uncertainty in the mapping of several degrees and the actual source region may be the lower coronal hole or it may be the active region between the two holes; in paper I we labeled this ARCH wind to indicate the ambiguity in the mapping.

Solar wind proton velocity, charge state density ratio O^{7+}/O^{6+} and iron to oxygen density ratio Fe/O (a low FIP to high FIP element ratio) for the period covering the three source regions is shown in Figure 6 (ACE days 345–370 of 1999). The ACE data are hourly averages except for Fe/O (3-hr average). The lines dividing the data into streams are taken from the mapping shown in Figure 5. Note that ACE longitude decreases with increasing time (Figure 3). The charge state ratio O^{7+}/O^{6+} in the solar wind has been found to be a good diagnostic of the temperature of the solar source region because of the relatively large abundances of O^{7+} and O^{6+} and because of the sensitivity of this ratio to temperature in the range of interest (von Steiger *et al.*, 1997; Hefti *et al.*, 2000). Figure 7, from von Steiger, Geiss, and Gloeckler (1997) shows the relationship between the density ratio O^{7+}/O^{6+} and the oxygen freezing-in temperature determined from this ratio, T_O.

In Figure 6, the solar wind from the large equatorial coronal hole centered at about 10° longitude (labeled CH1) can be seen at ACE on days 365–368. Note the high wind speed ($V \approx 700$ km s^{-1}) and very steady, low oxygen charge state ratio, $O^{7+}/O^{6+} \approx 0.05$, corresponding to a temperature of $T_O \approx 1.2$ MK (Figure 7). This is on the low end of coronal holes studies in Paper I in which coronal hole

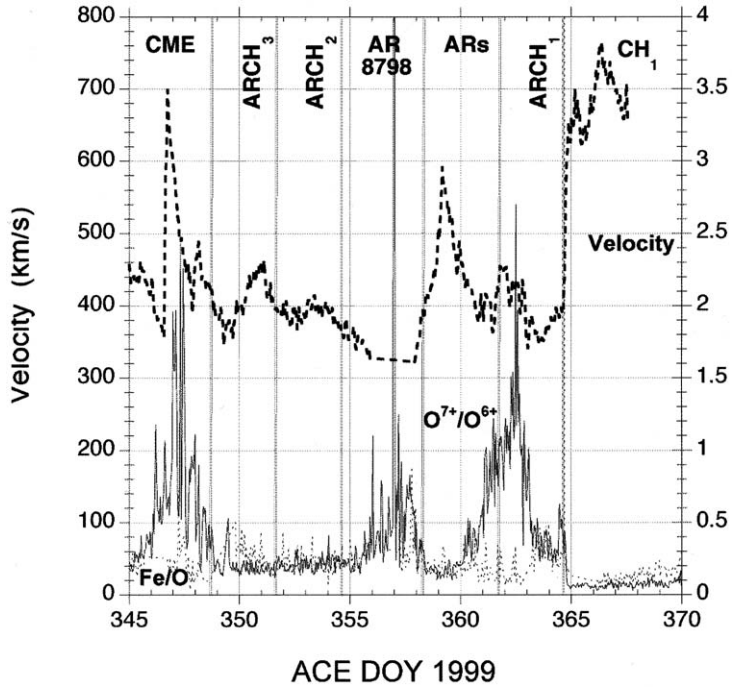

Figure 6. Solar wind data for ACE days 345–370 of 1999. Plotted are the proton velocity (*dot-dashed*) and the density ratios of O^{7+} to O^{6+} (*solid*) and of iron to oxygen (Fe/O, *dashed*). The Fe/O ratio is somewhat lower in the coronal hole (days 365–370) than in the other solar wind streams. See text for more discussion.

wind typically had $O^{7+}/O^{6+} < 0.2$ ($T_O < 1.6$ MK), but slightly higher than the ratio found in the large polar coronal holes at solar minimum ($O^{7+}/O^{6+} < 0.03$ or $T_O < 1.15$ MK) reported in von Steiger *et al.* (2000). In contrast, the O^{7+}/O^{6+} ratio in the wind from the AR 8798 active region is much higher $O^{7+}/O^{6+} \approx 0.2$–1 (corresponding to $T_O \approx 1.6$–2 MK) and highly variable. This is typical of active region wind identified in Paper I, which showed the ratio O^{7+}/O^{6+} in the range 0.1–0.6 (corresponding to $T_O = 1.4$–1.9 MK)(see also McComas *et al.*, 2001). Zurbuchen *et al.* (2000), analyzing the O^{7+}/O^{6+} ratio for 9 days of slow solar wind data in May 1998 found a similar range, $T_O \approx 1.5$–2 MK. In the indeterminate ARCH1 and ARCH2 regions, the wind speed is low ($V \sim 400$ km s^{-1}) and the O^{7+}/O^{6+} ratio is in a narrow range $O^{7+}/O^{6+} \approx 0.2$–0.3 ($T_O \approx 1.6$–1.7 MK), which is somewhat higher than typical CH values, but on the low end of active region values. This wind does not fall neatly into either the coronal hole or active region category; the ambiguity in the source has not been resolved.

Note that in the large high-speed coronal-hole wind (days > 365) the ratio Fe/O $\approx$ 0.1–0.2 is only slightly lower than in the ARCH regions (Fe/O $\approx$ 0.25) and in the active region (Fe/O > 0.25). At solar minimum, the density ratio Fe/O varies by about a factor of 2 between fast, coronal-hole wind and slow streamer-belt wind

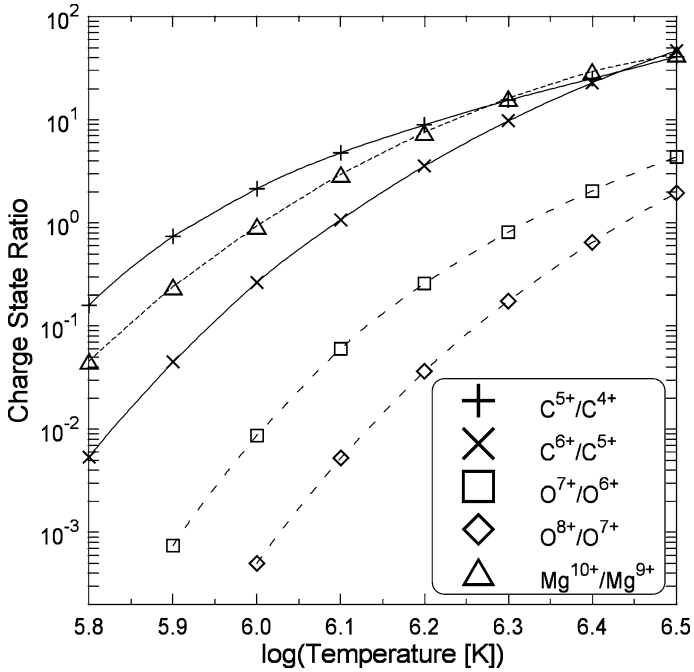

Figure 7. Oxygen freezing-in temperature as determined from the solar wind density ratio O^{7+}/O^{6+} (from von Steiger, 2003, private communication). This temperature is used as a proxy for the temperature of the source region of the wind because the ratio does not change as the solar wind propagates from the Sun to the spacecraft. From *Cosmic Winds and the Heliosphere*, edited by J.R. Jokipii, C. P. Sonett, and M. S. Giampapa, ©1997 the Arizona Board of Regents. Reprinted by permission of the University of Arizona Press.)

(Geiss, Gloeckler, and von Steiger, 1995; Geiss *et al.*, 1995; von Steiger *et al.*, 2000). Typically, at solar minimum Fe/O $\approx 0.05-0.07$ in fast wind and Fe/O $= 0.09-0.13$ in streamer belt wind (Plate 6 of von Steiger *et al.*, 2000). Thus, the Fe/O ratios seen in both coronal hole and active region wind in Figure 6 are typical of streamer belt wind near solar minimum.

The mapped ACE (in ecliptic) and *Ulysses* (about $-30°$ latitude) sources for CR1953 (18 August – 14 September 1999) are shown in Figure 8. For this rotation, we examine in detail at four ACE solar wind sources: (1) the small equatorial coronal hole at about 100° longitude; (2) the neighboring indeterminate ARCH wind stream spanning 120–170° longitude at the source surface, which may be from the strong field region or may be from the coronal hole just to the north; (3) the active-region stream spanning 180–240° longitude at the source surface, which emanates from AR 8681 and (4) the complex source region between 250° and 350° degrees which was sampled by both ACE and *Ulysses*. The ballistic mapping relation between ACE and *Ulysses* day number and solar longitude can be found in Figure 4 of Paper I. ACE solar wind data for the period of time covering the first three source regions is shown in Figure 9. The wind from the equatorial coronal

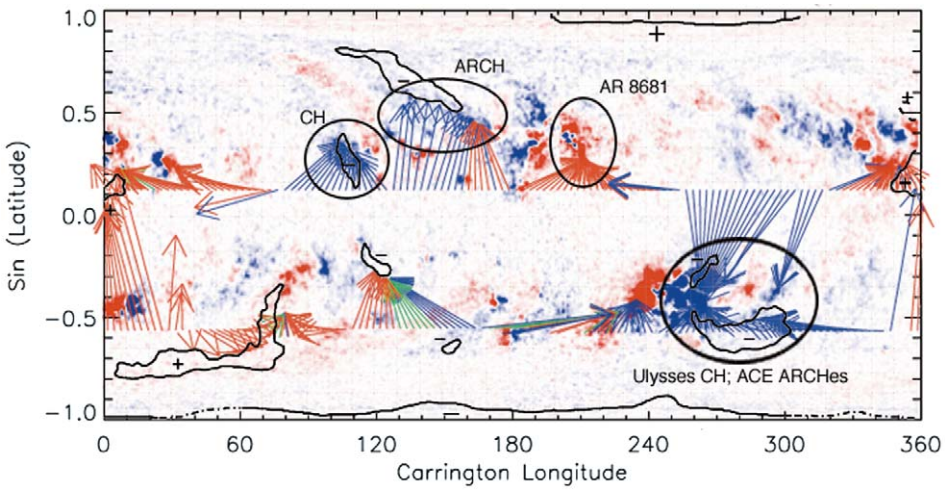

Figure 8. Mapping of spacecraft data from the source surface to the solar surface for CR1953. The arrow tail is the location at the source surface and the head is the footpoint at the solar surface.

hole (approximately ACE days 253–255) shows moderate speed (~ 500 km s^{-1}). Note in Figure 9 that the profile of the O^{7+}/O^{6+} ratio 'mirrors' the velocity profile, reaching a minimum of 0.1 (corresponding to $T_O = 1.4$ MK) where the velocity is maximum (520 km s^{-1}). Both the O^{7+}/O^{6+} minimum value (~ 0.1) and profile are typical of wind from the small coronal holes studied. The profile may result from mixing or interacting with neighboring wind streams or it may show a variation in temperature in the source region itself (Zurbuchen *et al.*, 1999). The earlier ARCH stream (days 250–253) shows very similar behavior, e.g., a minimum O^{7+}/O^{6+} ratio of 0.1 and a mirroring of the velocity profile. For this wind, the ambiguity in the mapping is removed and we can identify this stream as coronal hole wind. Note from Figure 8 that the AR8681 active region stream ($\sim$ days 243–247) shows large variations in the velocity and charge state data, suggesting multiple streams. The ratio O^{7+}/O^{6+} in this AR stream is generally higher than in the coronal hole wind, varying in range $O^{7+}/O^{6+} \approx 0.15$–$0.5$ ($T_O \approx 1.5$–1.9 MK).

Figure 9 also shows the ratio Fe/O and the average oxygen charge state $\langle Q \rangle_O$ (together with the O^{7+}/O^{6+} ratio). The 3-hour averaged Fe/O is rather variable in the range Fe/O ≈ 0.1–0.2 throughout this period, and, in this case, shows no particular difference between coronal hole and active region wind. As for the solar wind data in Figure 6, the Fe/O ratios seen in both coronal hole and active region wind near solar maximum is typical of streamer belt wind near solar minimum. The lower panel of Figure 9 shows that the profile of the average oxygen charge state, which uses the O^{7+} and O^{6+} data, is nearly identical to the O^{7+}/O^{6+} profile, but with some smoothing of the variations, presumably caused by statistical limitations to the data in the case of large O^{7+}/O^{6+}. From this data, we note that the minimum

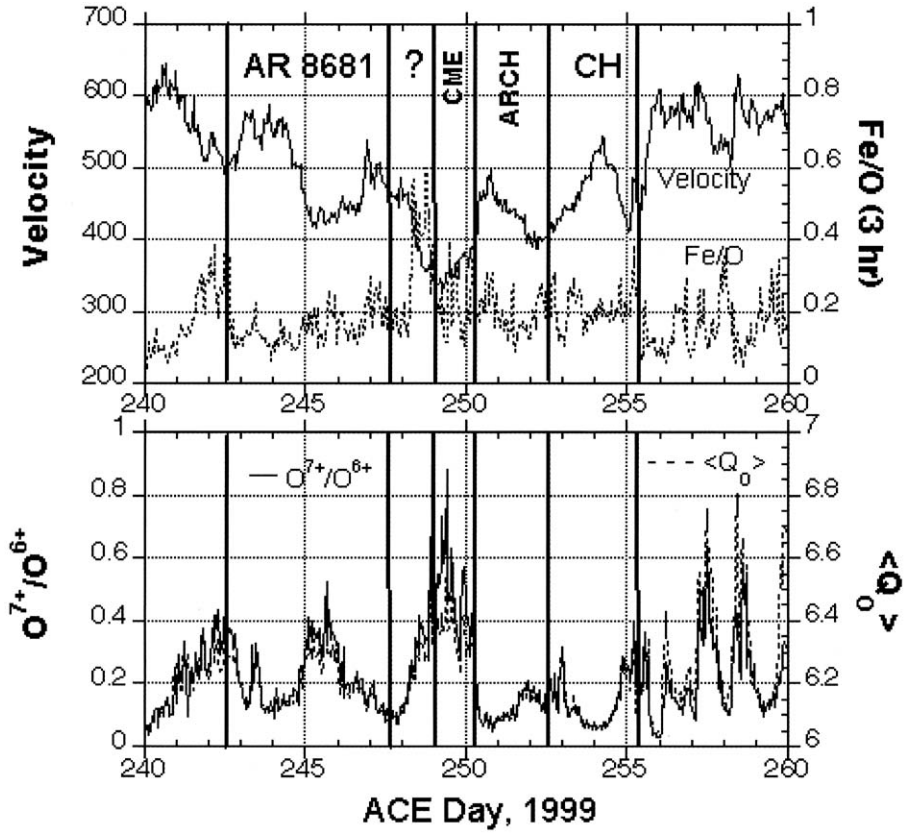

Figure 9. Upper: ACE proton velocity (*solid line*) and ratio of iron to oxygen Fe/O (*dashed line*). No systematic difference is seen in the Fe/O ratio in wind from different sources here. *Lower*: comparison of charge state ratio O^{7+}/O^{6+} (*solid line*) and average oxygen charge state $\langle Q_O \rangle$ (*dashed line*) illustrating how well the O^{7+}/O^{6+} ratio represents the average charge state computed from all oxygen charge state data. See text for more discussion.

oxygen charge state in the coronal-hole wind is $\langle Q \rangle_O \approx 6.05$ and that in stream from AR 8681 varies in the range $\langle Q \rangle_O \approx 6.1$–$6.4$.

Figure 10 compares solar wind data from a solar source area sampled by both ACE and *Ulysses* during CR1953. Shown are ACE (upper panel) and *Ulysses* (lower panel) velocities and oxygen charge state ratio O^{7+}/O^{6+} for the days when both spacecraft sampled solar wind that mapped to 200–360° at the source surface and to nearby source regions at the solar surface (see Figure 8). Note that *Ulysses* sampled this region about 30 days after ACE due to the difference in solar distance (4.6 AU for *Ulysses*) and longitude (about 200° separation). From Figure 8, it can be seen that ACE solar wind between 200–360° longitude at the source surface mapped to two neighboring source regions with coronal holes near active regions; these were classified as ambiguous ARCH sources in Paper I. The *Ulysses* solar wind between 200–360° longitude mapped to the moderate sized coronal hole

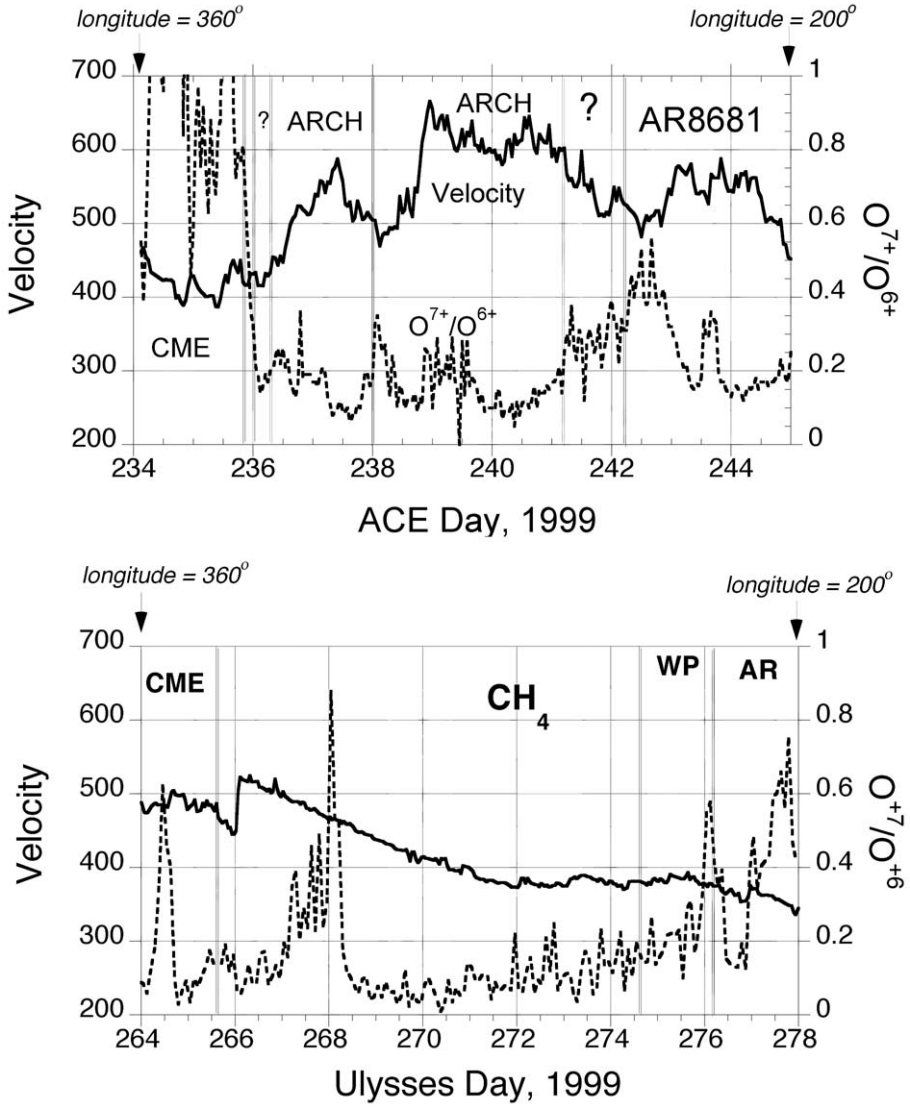

Figure 10. A comparison of solar wind data from ACE and *Ulysses* that maps to nearby sources on the solar surface. This wind maps to between 200–360° longitude at the source surface (see Figure 8). See text for a discussion.

centered at approximately 280° longitude; the source region was classified as a coronal hole in Paper I. In Figure 10 (lower panel), it can be seen that this wind has the O^{7+}/O^{6+} ratio characteristic of coronal-hole wind: $O^{7+}/O^{6+} < 0.2$ throughout with a minimum $O^{7+}/O^{6+} < 0.1$. The smaller ACE ARCH source (upper panel, day 237) is probably a coronal hole source since here also $O^{7+}/O^{6+} < 0.2$ throughout with a minimum $O^{7+}/O^{6+} < 0.1$ occurring at the velocity maximum

(600 km s^{-1}); this wind may well come from the same coronal hole as the *Ulysses* wind. The larger ACE ARCH source (days 238–240), which mapped to the edge of the *Ulysses* coronal hole, generally has $O^{7+}/O^{6+} < 0.2$, but because of the rather variable nature of the oxygen charge state ratio which exceeds 0.2 on day 239, the ambiguity remains.

In addition to the data presented in this paper, Liewer, Neugebauer, and Zurbuchen (2003) plotted some CR 1934 solar wind data (proton velocity and average oxygen charge state $\langle Q \rangle_O$ for ACE days 80–105 of 1998). This time period showed two wind streams from active-region sources and one equatorial coronal-hole stream with $V_{\max} \approx 600$ km s^{-1}. The findings regarding variations in the O^{7+}/O^{6+} ratio were similar to the cases above (Figures 6, 9, and 10): In the coronal hole, the minimum O^{7+}/O^{6+} ratio was ~ 0.05 (with the minimum value occurring at the time of the velocity maximum) whereas in the active-region stream, the ratio was higher and more variable, $O^{7+}/O^{6+} \approx 0.2–1.0$. The Fe/O ratio in the coronal-hole stream was fairly steady at about 0.1 whereas in the AR it was higher and more variable, Fe/O $\approx 0.1–0.3$. Thus, the results for CR1934 were consistent with those from C1953 and CR1957.

Note that the ratio in the large CH in CR 1957 was $O^{7+}/O^{6+} \sim 0.05$ with relatively fast wind ($V \sim 700$ km s^{-1}) (Figure 6).The minimum in the smaller coronal holes with slower wind (Figure 8) is $O^{7+}/O^{6+} \sim 0.1$, somewhat higher yet, but lower than that in the active regions (typically $O^{7+}/O^{6+} > 0.2$). Somewhat higher was the steady $O^{7+}/O^{6+} = 0.2–0.3$ in the indeterminate ARCH regions in Figure 6. These variations in the minimum O^{7+}/O^{6+} ratio support the suggestion in Paper I that there is perhaps a hierarchy of open field regions, with the large, polar coronal holes with very fast wind and very low source temperatures at one extreme, smaller, low-latitude coronal holes in the middle, and open flux in active regions at the other extreme.

4. Comparison of Active Region Source Structure with Coronal Images

In this section, we compare the magnetic topology of the active-region sources with *Yohkoh* soft X-ray and SOHO/EIT EUV images of the corona to look for signatures of the active region open flux in the coronal images. Levine *et al.* (1977) also using PFSS models, found open flux associated with active regions that did not have corresponding *Skylab* coronal holes. Those open flux regions often had corresponding dark features in *Skylab* soft X-ray images (and often they evolved into *Skylab* coronal holes). Here we address the question whether the active-region sources we identified, which do not have corresponding coronal holes in the synoptic He 10840 Å coronal hole maps, have corresponding dark features in the EUV and/or soft X-ray. We find that most, but not all, AR sources do have corresponding dark features. The one exception is discussed first.

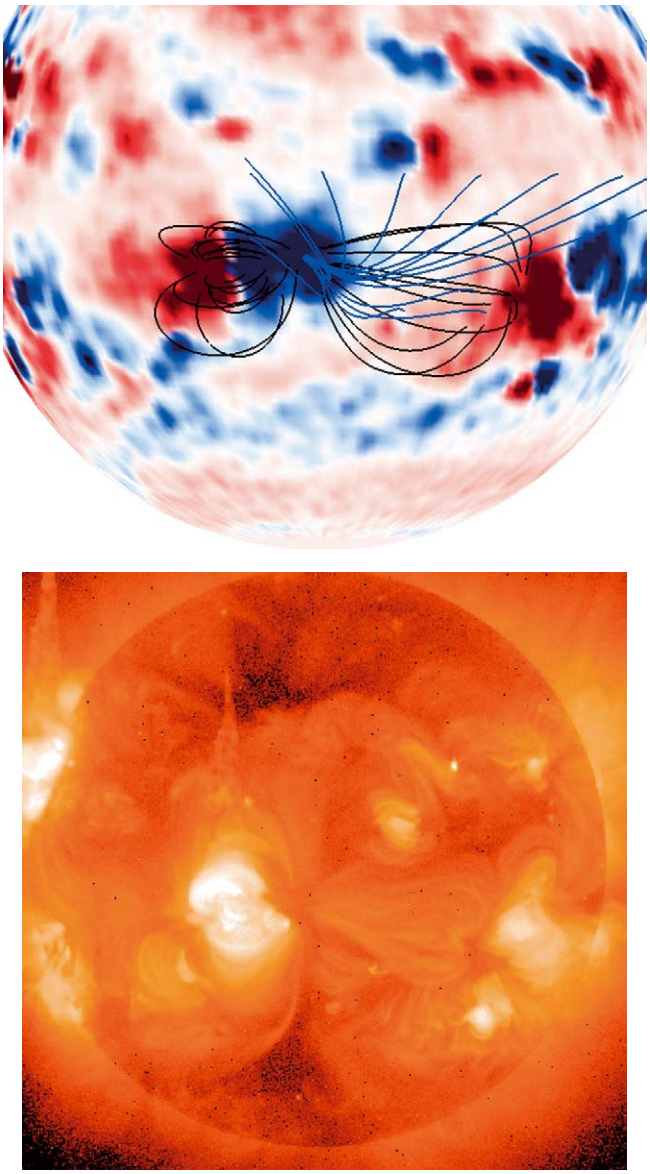

Figure 11. Top: PFSS magnetic model of AR 8798. Some closed field lines (*black*) connect to the opposite polarity region of a second bipolar region. The open (*blue*) field lie near the separatrix between loops connecting to the different opposite polarity regions. *Bottom: Yohkoh* soft X-ray image of AR 8798 (left of disk center) from the same view point (18 December 1999) showing the field lines connecting to the second bipolar region. The image confirms the double dipole structure, but shows no dark feature at the location of the open flux.

The upper image in Figure 11 shows both open (blue) and closed (black) magnetic field lines for the PFSS model of AR 8798, oriented as viewed from Earth on 18 December 1999 (CR 1957, same view as in Figure 1). This active-region bipole (slightly left of disk center) is part of a double dipole complex: some of the field lines from one polarity (blue = inward) of the active region bipole connect to the opposite polarity region of the second dipole (right of disk center). Open flux originates near the separatrix (from the 'cowlick') that separates field lines connecting to the two different opposite polarity regions. The open field lines shown include those that map to the ACE spacecraft. The lower image in Figure 11 shows the corresponding *Yohkoh* soft X-ray image for 18 December 1999. Active region AR 8798 is evident as the bright loops slightly left of disk center. The image clearly shows both the bright field lines that connect within the active region dipole and the field lines that connect in the opposite direction to the second dipole. Thus the soft X-ray image confirms the double dipole nature of the region. The separatrix (the 'part' in the loops) associated with the open flux is clearly evident in the soft X-ray loops, but the open flux is not evident as a dark feature or lane. To our knowledge, we are the first to report this morphology – open flux within an active region with no dark feature. Note that whether or not a dark lane can be seen is dependent on the viewing geometry since other loops in the line of sight might obscure it. In this case, however, we are viewing the separatrix directly 'down the barrel' and this is not an issue.

The magnetic structure of AR 8681 in CR 1953 is investigated in Figure 12. The upper image in Figure 12 shows the PFSS model field lines (colored as in Figure 1) as viewed from Earth 28 August 1999. Also shown in black are closed field lines of AR8681. Below is the corresponding SOHO EIT 284 image for the same day. The yellow lines are closed loops from the PFSS model; the gray field lines are those that connect to ACE. Comparison with the model indicates that the large dark corridor lies below expanding open flux that originates, not in the dark region, but from the strong field regions to the north and south. This is the topology of the dark corridors between loop complexes in Švestka *et al.* (1977) and this topology was found for the active-region solar wind source in CR1934 described in Liewer, Neugebauer, and Zurbuchen (2003). The open flux from AR 8193 originated near the outer edge of the active-region bipole and expanded out over a neighboring dark corridor. Thus we find that the dark corridor seen in the EUV image indicates open flux, but here the mapping suggests that open flux footpoints lie in or near the neighboring strong field regions, not the dark region itself.

5. Conclusions and Discussion

The work presented here used magnetic models, solar wind data and soft X-ray and EUV images of the Sun to give a detailed description of several active-region sources of solar wind near solar maximum. We found that the solar wind O^{7+}/O^{6+}

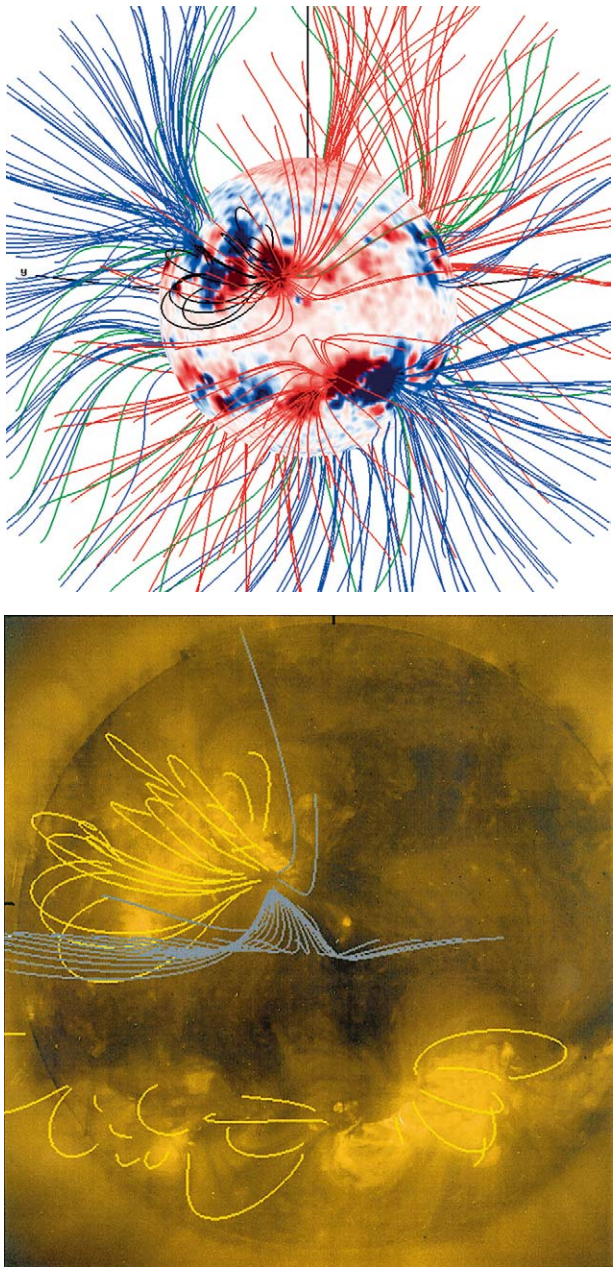

Figure 12. Top: PFSS coronal model of CR 1953 with closed field lines of AR,8681 shown as *black lines*, as viewed on 28 August 1999. *Bottom*: SOHO EIT 284 image for the same day showing a very large dark lane lying under the open flux from the strong field regions to the north and south. Superimposed are magnetic field lines from the PFSS model; *yellow lines* are closed field lines and *gray lines* are the open field lines from the edge of the active region that connected to ACE.

density ratio in wind from active regions shows different signatures than in wind from coronal holes. (Recall our definition of active-region source: strong-field region with no corresponding coronal hole in the NSO He 10830 Å synoptic coronal hole maps.) Active-region wind studied here typically shows higher and more variable ratios, $O^{7+}/O^{6+} \approx 0.2–0.6$, corresponding to an oxygen freezing in temperature of $T_O \approx 1.6–1.9$ MK. The higher oxygen freezing in temperature indicates that the source region temperature is higher. The wind from active regions may have been heated on closed field lines that opened by reconnection, allowing the plasma to escape. Such an interpretation is consistent with that of Zurbuchen *et al.* (2000) who concluded that slow wind with higher charge states emerges from closed coronal magnetic structures. The concept of solar wind resulting from the opening of loops as been further developed (Fisk, 2003, and references therein). The variability may result from different flux tubes reconnecting. We note that Feldman, Widing, and Warren (1999) in their study of the morphology of coronal loops, found that at solar maximum, there was a class of long, high loops with temperatures in the 1–1.4 MK range that connected different active regions and which tend to be colder than loops connecting within a single active region. It may be the opening of loops such as these which gives rise to the AR wind identified here. This could explain why the source temperatures of active region wind reported here and in Paper I are lower than the temperature of typical active region plasma ($T > 2$ MK).

In contrast to the highly variable O^{7+}/O^{6+} profile of AR wind, coronal-hole wind typically shows a smooth profile with a minimum occurring near the velocity maximum. The minimum value is $O^{7+}/O^{6+} < 0.2$, corresponding to an oxygen freezing in temperature $T_O < 1.6$ MK. This is somewhat higher than the values for fast wind at solar minimum, which typically has $T_O < 1.2$ MK. The O^{7+}/O^{6+} profile may result from mixing or stream–stream interactions or it may result from a variation in the temperature across the source region (Zurbuchen *et al.*, 1999).

However, not every solar wind stream can be classified as either coronal-hole or active-region wind on the basis of the mapping and the O^{7+}/O^{6+} data. We also found ambiguous cases, e.g., ARCH cases where the O^{7+}/O^{6+} ratio was fairly steady, but in the overlap region between coronal-hole and active-regions sources, $O^{7+}/O^{6+} \approx 0.2–0.3$ ($T_O \approx 1.6–1.7$ MK). Thus, our results are consistent with the contention in Paper I that there is perhaps a hierarchy of open field regions, with the large, polar coronal holes with very fast wind and very low source temperatures at one extreme, smaller, low-latitude coronal holes in the middle, and open flux regions in active regions at the other extreme.

A comparison of the magnetic field topology with soft X-ray and EUV data showed that, in all cases studied, the open flux predicted by the PFSS mode was evident in and consistent with the active-region images. In most of the active-region sources studied, reported here and in Liewer, Neugebauer, and Zurbucher (2003), the open field lines were from the edge of the active region and a dark feature or corridor was seen as in Levine *et al.* (1977) and Švestka *et al.* (1977).

However, in one case shown here, no dark feature was evident in the soft-X ray images: the magnetic model showed a double dipole coronal structure consistent with the images, both indicating that the footpoints of the open field lines, rooted deep within the active region, lay near the separatrix between loops connecting to two different opposite polarity regions.

In Luhmann *et al.* (2002) it was found that the appearance of open flux in mid and low latitudes was related to the appearance of active regions. Note that our active-region sources are not equivalent to the 'active-region holes' discussed in Luhmann *et al.* (2002). In that paper, the term 'active-region holes' was used to describe open flux from active region latitudes, but whose footpoints did not necessarily lie in strong field regions. Schrijver and DeRosa (2003) have shown, however, that at solar maximum 40% of the heliospheric open flux comes from active regions (areas with a flux intensity > 50 Mx cm^{-2}).

What is a coronal hole? In broad terms, a coronal hole is generally considered to be a region of low emissivity in the corona indicating a density depletion and/or lower temperature. Levine (1982) stressed the importance of keeping a distinction between 'open flux' and 'coronal hole' because the definition of a coronal hole is an observational one. A discussion and history of usage of the term coronal hole can be found in Schrijver and DeRosa (2003). In cases of long-lived, sizeable coronal holes that can be identified in both NSO 10830 Å coronal hole maps and in EUV or soft X-ray images, it is clear when there is a coronal hole. Often narrow X-ray/EUV coronal holes, which may or may not be seen in 10830 Å coronal hole maps, can only be seen when at disk center due to projection and line-of-sight effects. It has generally been assumed that coronal holes are rooted in unipolar regions. However, our results, as well as those of others (Levine *et al.*, 1977; Kojima *et al.*, 1998; Luhmann *et al.*, 2002; Schrijver and DeRosa, 2003; Arge *et al.*, 2003) show that there is solar wind coming from open flux in or near active regions. We have shown here and in Paper I that solar wind from open flux within active regions has different properties from the wind of the traditional coronal holes. We have found that the observed range of oxygen freezing-in temperatures for coronal holes and active regions overlaps and some source regions are ambiguous, suggesting that there may be a continuous distribution of open flux solar wind source regions with the large coronal holes with fast wind and low ionization temperature at one extreme and the hotter, active region open flux areas at the other extreme. In one active-region source studied here, open flux was not associated with the dark area in coronal images, but with double bipolar magnetic topology consistent with open flux rooted deep within an active region. Thus we advocate (as do Schrijver and De Rosa, 2003) that not all open flux regions should be called 'coronal holes'. Rather, coronal holes (low emissivity regions identified in soft X-ray and/or EUV) form a large subset of possible open magnetic field structures in the corona. This is equivalent to the assertion in Levine (1977) that open flux is a necessary, but not sufficient, condition for a coronal hole. If 'coronal hole' and 'open flux' are treated as synonyms, then one must note that, not only are some 'coronal holes'

not evident in soft X-ray and/or EUV images, but also that some 'coronal-hole' wind has properties like slow 'streamer'-wind at solar minimum.

Acknowledgements

We thank Z. Mikiċ for the potential magnetic field and field line tracing programs used in this work. We also thank E. J. Smith, J. Luhmann, Y.-M. Yang, N. Sheeley, K. Schrijver, L. Fisk, and D. McComas for useful discussions. NSO/Kitt Peak magnetograms and coronal hole data used here are produced cooperatively by NSF/NOAO, NASA/GSFC, and NOAA/SEL. The solar images used here are from the Soft X-ray Telescope (SXT) instrument on the *Yohkoh* spacecraft, a cooperative mission of Japan, the USA, and the UK, and from the EIT instrument on SOHO, a joint ESA-NASA mission. Much of this work is the result of research performed at the Jet Propulsion Laboratory of the California Institute of Technology under a contract with the National Aeronautics and Space Administration. The University of Michigan work was supported, in part, by NASA grant NAG5-10975 and NASA-JPL contract 955460.

References

Arge, C. N., Harvey, K. L., Hudson, H. S., and Kahler, S. W.: 2003, in M. Velli, R. Bruno, and F. Malara, (eds.), *Solar Wind Ten: Proceedings of the Tenth Intl. Solar Wind Conference*, AIP, NY, p. 202.

Feldman, U., Widing, K. G., and Warren, H. P.: 1999, *Astrophys. J.* **522**, 1133.

Fisk, L. A.: 2003, *J. Geophys. Res.* **108**, 1157.

Geiss, J., Gloeckler, G., and von Steiger, R.: 1995, *Space Sci. Rev.* **72**, 49.

Geiss, J., Gloeckler, G., von Steiger, R., Balsiger, H., Fisk, L. A., Galvin, A. B., Ipavich, F. M., Livi, S., McKenzie, J. F., Ogilvie, K. W., and Wilken, B.: 1995, *Science* **268**, 1033.

Hefti, S., Grunwaldt, H., Bochsler, P., and Aelig, M. R.: 2000, *J. Geophys. Res.* **105**, 10527.

Kojima, M., Fujiki, K., Ohmi, T., Tokamaru, M., Yokobe, A., and Hakamada, K.: 1999, *J. Geophys. Res.* **104**, 16993.

Levine, R. H.: 1977, *Astrophys. J.* **218**, 291.

Levine, R. H.: 1977, in J. B. Zirker (ed.), *Coronal Holes and High Speed Wind Streams*, Co. Assoc. Univ. Press, Boulder, p. 103.

Levine, R. H.: 1982, *Solar Phys.* **79**, 203.

Liewer, P. C., Neugebauer, M., and Zurbuchen, T.: 2003, in M. Velli, R. Bruno and F. Malara (eds.), *Solar Wind Ten: Proceedings of the Tenth Intl. Solar Wind Conference*, AIP, NY, p. 51.

Luhmann, J. G., Li, Y., Arge, C. N., Gazis, P. R., and Ulrich, R.: 2002, *J. Geophys. Res* **107**, A8, SMP 3-1, CiteID 1154.

McComas, D. J., Gosling, J. T., and Skoug, R. M.: 2000, *Geophys. Res. Lett.* **27**, 2437.

McComas, D. J., Goldstein, R., Gosling, J. T., and Skoug, R. M.: 2001, *Spac. Sci. Rev.* **97**, 99.

McComas, D. J., Elliott, H. A., and. von Steiger, R.: 2002, *Geophys. Res. Lett.* **29**, 10.1029/2001GL013940.

Neugebauer, M., Forsyth, R. J., Galvin, A. B., Harvey, K. L., Hoeksema, J. T., Lazarus, A. J., Lepping, R. P., Linker, J. A., Mikic, Z., Steinberg, J. T., von Steiger, R., Wang, Y.-M., Wimmer-Schweingruber, R. F.: 1998, *J. Geophys. Res.* **103**, 14587.

Neugebauer, M., Liewer, P. C., Smith, E. J., Skoug, R. M., and Zurbuchen, T. H.: 2002, *J. Geophys. Res.* **107**(A12) SSH13-1, CiteID 1488 (Paper I).

Schrijver, C. J. and DeRosa, M. L.: 2003, *Solar Phys.* **212**, 165.

Švestka, Z., Solodyna, C. V., Howard, R., and Levine, R. H.: 1977, *Solar Phys.* **55**, 359.

von Steiger, R., Geiss, J., and Gloeckler, G.: 1997, in J. R. Jokipii, C. P. Sonett, and M. S. Giampapa, (eds.), *Cosmic Winds and the Heliosphere*, University of Arizona Press, Tucson, pp. 581–616.

von Steiger, R., Zurbuchen, T. H., Geiss, J., Gloeckler, G., Fisk, L. A., and Schwadron, N. A.: 1997, *Space Sci. Rev.* **97**, 123.

von Steiger, R., Schwadron, N. A., Fisk, L. A., Geiss, J., Gloeckler, G., Hefti, S., Wilken, B., Wimmer-Schweingruber, R. F., and Zurbuchen, T. H.,: 2000, *J. Geophys. Res* **105**, 27217.

Wang, Y.-M. and Sheeley, N. R., Jr.: 1997, *Geophys. Res. Lett.* **24**, 3141.

Wang, Y.-M. and Sheeley, N. R., Jr.: 2003, *Astrophys. J.* **587**, 818.

Wang, Y.-M., Sheeley, N. R., Jr., Howard, R. A., Kraemer, J. R., Rich, N. B., Andrews, M. D., Brueckner, G. E., Dere, K. P., Koomen, M. J., Korendyke, C. M., Michels, D. J., Moses, J. D., Paswaters, S. E., Socker, D. G., Wang, D., Lamy, P. L., Llebaria, A., Vibert, D., Schwenn, R., and Simnett, G. M.: 1997a, *Astrophys. J.* **485**, 875.

Wang, Y.-M., Sheeley, N. R., Jr., Walters, J. H., Brueckner, G. E., Howard, R. A., Michels, D. J., Lamy, Schwenn, R., and Simnett, G. M.: 1997b, *Astrophys. J.* **498**, L165.

Wang, Y.-M., Sheeley, N. R., Jr., Walters, J. H., Brueckner, G. E., Howard, R. A., Michels, D. J., Lamy, P. L., Schwenn, R., Simnett, G. M.: 1998, *Astrophys. J.* **498**, L165.

Zurbuchen, T. H., Hefti, S. Fisk, L. A., Gloeckler, G., and von Steiger, R.: 1999, *Space Sci. Rev.* **87**, 353.

Zurbuchen, T. H., Hefti, S., Fisk, L. A.,, Gloeckler, G., and Schwadron, N. A.: 2000, *J. Geophys. Res.* **105**, 18327.